This is a repository copy of *The mutual interaction between tribochemistry and lubrication: Interfacial mechanics of tribofilm*.

The mutual interaction between tribochemistry and lubrication: Interfacial mechanics of tribofilm

Abdullah Azam, Abdel Dorgham, Pourya Parsaeian, Ardian Morina, Anne Neville, Mark C.T. Wilson

Institute of Functional Surfaces,
School of Mechanical Engineering, University of Leeds, Leeds, UK

Abstract

A new mechanism for the action of antiwear tribofilms is proposed. The antiwear action of ZDDP additive is believed to be mainly due to the formation of tribofilms that reduce wear by chemical action. In this study, a mixed lubrication model is developed and tribofilm growth integrated into this model to simulate the effects of tribofilms on lubrication. The dynamic evolution of the contacting surfaces due to plastic deformation, wear and tribofilm growth continuously change the lubrication characteristics inside the contact. It is observed that the growth of tribofilm roughens the contact and increase contact severity. It was found that this roughness increase also helps to entrain more lubricant, resulting in thicker lubricant films. Therefore, the plot of the evolution of film thickness ratio ($h_{central}(t)/R_q(t)$) shows that the lubrication regime is improved by the presence of tribofilm. Therefore, not only the chemical presence but the physical presence of the tribofilm on the surfaces also helps to improve contact performance by retaining more lubricant and improving the lubrication regime.

Keywords: `mixed lubrication, tribofilm, ZDDP, lambda ratio, roughness evolution.`

1. Introduction

Friction and wear are reduced by providing lubricant to the contact. Lubricants operate by providing a slippery interface under normal conditions but under extreme conditions, the contact goes into the mixed lubrication regime with distinct solid and lubricated contact regions and finally into the boundary lubrication regime with no effective lubricant film. Protection under such conditions is provided by the addition of chemical additives in the lubricant. These additives are passively present within the lubricant and

supply on demand protection under high shear conditions by forming thick tenacious layers that reduce wear by several mechanisms [1]. There has been a lot of research ongoing to study the formation, removal, mechanism of action and the nature of these tribofilms. Recently, more efforts are being made to understand the transient behaviour of formation of these films [2, 3].

The first successful EHL solution was presented by Petrusevich in 1951 [4]. Ever since, the study of EHL has continuously evolved for the last 60 years. The EHL and boundary lubrication regimes can be considered as special cases of mixed lubrication regime. Initially smooth surface point contact EHL solutions were presented by Ranger et al. [5] and then by Hamrock and Dowson [6, 7] in a series of papers. Several refined models were developed later to access higher loads [8, 9, 10], thermal EHL [11, 12], use of multigrid methods [13, 14, 15, 16], transient effects [17] and the inclusion of Non-Newtonian effects [18, 19, 20, 21, 22]. Roughness was first included, in point contact EHL solutions, stochastically by Zhu and Cheng [23]. Based upon this, the first deterministic rough surface EHL model was given by Chang et al. [24]. None of these studies considered asperity contacts.

The first mixed lubrication model (an EHL model with asperity contacts incorporated) was first presented by Jiang et al [25] based upon the separate approach where the asperity contacts and lubricant flow are solved separately. Using this approach about 12 % solid contact area ratio could be achieved. The unified EHL solution method was presented by Zhu and Hu [26] and then by Holmes et al. [27] to solve the mixed lubrication problem in gear applications. Li and Kahraman [28] presented a unified solution algorithm based upon the asymmetric integrated control volume approach to overcome the issue of grid dependence of EHL solutions [29]. The basic idea in unified solution algorithm is to solve the asperity and lubricated contacts by using only the Reynolds equation. This method can give detailed contact pressure and film thickness values that can be used to extract macro-scopic system variables like friction, flash temperature and surface and subsurface stresses.

The unified algorithm has been improved in many ways over the last 15 to 20 years. Wang et al. [30] implemented the DC-FFT to solve the deformation convolution. This improved the calculation efficiency significantly. The mesh dependence of EHL solution algorithms was addressed by Liu et al. [29]. Zhu [31] provided detailed discussion on the use of a limiting value of lubricant film thickness to define contact and suggested a range of acceptable mesh densities. Wang et al. [32] compared the solutions from unified algorithm using Reynolds equation with the boundary lubrication solvers to further consolidate the unified modelling approach. Inclusion of interasperity cavitation was presented by Wang et al. [33] by combining the concepts of fractional film defect given by Jacobsson and Flodeberg [34] and the mass

2

conserving algorithm proposed by Elrod [35].

In engineering components, several complex phenomenon are simultaneously taking place at the tribological interfaces, requiring integration of several branches of science. The ultimate goal is to include advanced theories to simulate such complex interfaces by releasing the assumptions one by one. A need for such a model, enabling the study of complex interfacial phenomenon, was suggested recently by Zhu and Wang [36]. They suggest that the link between the micro- and nano-scale properties of interfaces and the macroscopic contact performance parameters like friction and wear is missing. Therefore, a multiscale engineering model capable of establishing this link is greatly needed.

The current study builds upon the author's recent work on the tribochemical film growth model [37, 38]. The continuum restriction is overcome by approximating tribochemical film growth as an empirical equation. Integrating the science of lubrication, contact mechanics and tribochemistry enables not only the study of contact parameters on lubrication parameters but also vice versa. Models that can enable the study of such complex phenomenon are the need of time.

The current paper, therefore, studies the effect of presence and build up of the antiwear tribofilms on the key lubrication parameters using the multiscale engineering model that combines contact mechanics, lubrication and tribochemistry in a clever way. The results from the current study unfold a new mechanism of action of the antiwear additive ZDDP. To date, there has been no study dealing with this issue and this is the first attempt to capture the interfacial mechanics of the tribofilm growth by linking these difference sciences.

This paper is organized by first introducing the model components and then presenting a brief summary of the numerical implementation details. Finally, the results for representative cases, with and without the inclusion of tribofilm, are presented and discussed within the scope of action of the antiwear additive ZDDP.

2. The complete tribochemical mixed lubrication model

A tribological contact is realized between a rough spherical ball and rough disc. Rough surfaces are generated using in-house code written in Matlab which is based upon the method of Tonder et al. [39]. Both the macro- and micro-geometries are considered in this contact. The contact between the two rough surfaces is solved to get the contact pressures and film thickness distribution inside the contact. In the following, first the mixed lubrication model is detailed and then the tribochemical model is outlined. The integration of

3

these two models and the solution procedure have been presented elsewhere [37, 40] but details are provided in the following sections for completeness.

2.1. Mixed lubrication model

The mixed lubrication problem can be effectively solved by using the the Reynolds equation, the film thickness equation and the load balance equation along with the two equations of state relating the density and viscosity of the lubricant to pressure. First of all a mixed lubrication model is developed and then the plastic deformation model is implemented. The model developed in this work is based upon the semi-system approach [14] where terms from both the pressure flow and entrainment flow parts of the Reynolds equation are used to build the coefficient matrix. This ensures that the diagonal dominance is maintained under extreme conditions when the pressure flow terms become insignificant. The Reynolds solver based solely upon the pressure flow terms is likely to suffer from slow convergence or no convergence at all especially when under high load cases with high frequency roughness. It has been suggested by Hu and Zhu [41] that the pressure flow terms can be turned off when the lubricant film thickness reduces to negligibly small values. This approach enables the solution of the EHL and mixed lubrication problems in a unified manner. Therefore, both the lubricant and solid contact pressures can be calcualted using the Reynolds equation alone. The flow obstructions arising when solving the Reynolds equation for rough surface contacts (asperity contacts) manifest themselves in the form of a very small local film thickness. At the computational nodes where the lubricant film thickness falls below a certain predefined value (1 nm in this study), the reduction of the pressure flow terms in the Reynolds equation to negligible values represents obstructions to the flow. In the current study, the Reynolds solver based upon the semi-system and the unified algorithm is robust enough to generate lubricant and solid pressures in a single framework. The algorithm to calculate plastic deformation within the lubricated contact will be explained in the next sections while a brief summary of the equations describing the EHL and mixed lubrication system is presented next.

The complete pressure profile is computed by solving the Reynolds equation, given as

$$\frac{\partial}{\partial x}\left[\left(\frac{\rho h^3}{12\eta}\right)\frac{\partial p}{\partial x}\right] + \frac{\partial}{\partial y}\left[\left(\frac{\rho h^3}{12\eta}\right)\frac{\partial p}{\partial y}\right] = \left(\frac{u_1 + u_2}{2}\right)\frac{\partial(\rho h)}{\partial x} + \frac{\partial(\rho h)}{\partial t} \qquad (1)$$

In this equation, the variables h, ρ and η represent lubricant film thickness, density and viscosity, respectively. The pressure, speed of body 1 and speed of body 2 are represented by p, u_1 and u_2 where as x, y and t are the

4

spatial and time variables. The lubricant properties are described through its viscosity. The current study assumes the fluid to be Newtonian and the flow direction is aligned to the x-coordinate. Two boundary conditions are applied. At the boundaries of the solution domain, $p = 0$ is applied. The diverging region formed at the exit of the EHL and mixed lubricated contact is prone to cavitation due to the pressure in this region falling below the fluid vapour pressure [42]. The Swift-Steiber boundary condition is applied to handle cavitation by enforcing the pressure beyond cavitation boundary, x_e to be zero i.e. $\{\forall x \geq x_e, p < 0 \Rightarrow p = 0\}$

The film thickness equation for the point contact is expressed as

$$h = h_0(t) + \frac{x^2}{2R_x} + \frac{x^2}{2R_y} + v_{e+p}(x, y, t) + \delta(x, y, t) \tag{2}$$

The film thickness is also termed as gap as it defines the relative gap between mating surfaces. This equation describes the point contact. The v_{e+p} describes the total deformation. It includes an elastic as well as plastic part. The algorithm implemented in this study to deal with plastic deformation is based upon the authors previously published work [40]. At this stage, within the mixed lubrication solver, the deformation cannot be separated into individual components. The details on how to extract the plastic deformation will be presented in the next section. The term $h_0(t)$ defines the undeformed gap where as the term $\frac{x^2}{2R_x} + \frac{x^2}{2R_y}$ and $\delta(x, y, t)$ represent the macro-geometry and the micro-geometry (deterministic roughness), respectively. The surface elastic deformation is represented by the famous Boussinesq integral formulation:

$$v_{e+p} = \frac{2}{\pi E'} \int \int_\sigma \frac{p(x, y)}{\sqrt{(x' - x)^2 + (y' - y)^2}} dX dY \tag{3}$$

It is to be pointed out at this stage that for loads which are likely to cause plastic deformation, the elastic deformation will be unrealistically large. Equation 6 is non-dimensionalised and converted into discrete form to get the deformation matrix.

$$V_{ij} = 2\frac{\Delta X}{\pi^2} \sum_{k=1}^{M} \sum_{l=1}^{N} D_{ij}^{kl} P_{kl} \tag{4}$$

In this equation, the matrix D_{ij}^{kl} is called the flexibility matrix and the pressure $P_{kl} = \frac{p_{kl}}{P_h}$ where P_h denotes the Hertzian pressure. The matrix D_{ij}^{kl} forms a convolution with pressure P_{kl} which can be solved more efficiently using Fast Fourier Transforms (FFTs). The use of FFTs makes the solution process much quicker and makes denser grids accessible.The deformation matrix

is written as convolution

$$V(X_i, Y_j) = \sum_{k=1}^{M-1} K(X_i - X_k, Y_j - Y_k) * P(X_k, Y_k) \qquad (5)$$

The application of FFTs require the conversion of this linear convolution to a cyclic convolution by pre-treating the pressure matrix and the flexibility matrix [43]. The Direct Convolution - FFT method is computationally much more efficient compared to the other methods for calculation of surface deformation [30]. The viscosity in an EHL contact is considered as a function of pressure and the Roelands equation is used to describe it.

$$\eta(p) = \exp\left(\ln(\eta_0) + 9.67\right)(-1 + (1 + \frac{P_H}{p_0}p)^z) \qquad (6)$$

In this equation, the term η_0 describes the viscosity at ambient conditions and the exponent z is called the Roelands pressure viscosity index. It is a dimensionless parameter obtained through curve fitting. The calculations in the current study are based upon a value of $z = 0.68$. The lubricant density is also considered a function of pressure only and is calculated using the following equation,

$$\rho = \rho_0(1 + \frac{0.6 X 10^{-9}p}{1 + 1.7 X 10^{-9}p}) \qquad (7)$$

The final equation is the load balance equation which in the non-dimensional form is represented as,

$$\sum_{x_i, y_i}^{x_o, y_o} P(X, Y)dXdY = \frac{2\pi}{3} \qquad (8)$$

where the i and o indices correspond to the inlet and outlet of the solution domain.

The five equations (equation 1 to 8) form a complete set of equations. The solution to this set of equations gives the pressure and film thickness profiles. The equation set presented above is highly non-linear in character and a robust numerical solution procedure is required. The equations are solved in an iterative manner. A solver based upon the tridiagonal matrix algorithm (TDMA) is designed where finite difference discretization is applied to the Reynolds equation. The terms on the left hand side of equation 1 are called the pressure flow terms. These are discretized using the central difference approach. The terms on the right hand side of equation 1 are called the entrainment flow terms. These are discretized using first order backward differences. The resulting discretized equation is formulated in the form of

6

a linear algebra problem $AY = B$ where A is the coefficient matrix of the order $N \times N$. In the current study, the coefficient matrix is built from the pressure flow as well as the entrainment flow terms. The vector Y contains the unknown values. For a line contact problem only one system of equations $AY = B$ is solved but for a point contact problem, a series of systems of equations $AY = B$ is solved. The solution process uses a direct iterative approach which takes the flexibility of the iterative solvers and the accuracy of the direct solvers. A relaxation factor of 0.2 is used where the pressure update takes only 20 % of the new guess values while 80 % of the old guess values. This ensures that the solution moves slowly from the initial guess towards the final guess. The convergence criteria for the pressure loop was kept between 5×10^{-5} and 5×10^{-4} while the convergence criteria for the load balance condition was fixed at 1×10^{-4}. The pressures predicted by the Reynolds solver update the flexibility matrix which is again used to update the coefficient matrix for Reynolds solver again. Therefore, repeating this procedure, converged pressure and film thickness values can been obtained. It was found, in the current study, that change in the lubricant film thickness predictions was less than 1 % when the mesh density was refined from 128 $\times$ 128 to 256 $\times$ 256. Therefore, a mesh density of 128 $\times$ 128 is employed. Liu et al. [29] also found that this mesh density is sufficient to get desired accuracy.

2.2. Plastoelastohydrodynamic lubrication (PEHL) model

The deformation obtained from the previous step is still elastic. It may be elasto-plastic if the pressure exceeds the average yield stress of the material. In that case, the deformation predicted by the Boussinesq formulation (equation 6) will be unrealistically high. Therefore, a method was developed by the authors was developed to extract the plastic deformation magnitude from the elasto-plastic deformation [40].

The key idea behind the plastic deformation algorithm used int he current study is that the nodes that deform plastically float on the surface to form a plane. A computational node is considered to be undergoing elasto-plastic deformation if the pressure at that node reaches or exceeds the average yielding pressure (hardness of material). Therefore, if a node is experiencing plastic deformation, the pressure at that node is limited to the yielding pressure. This limiting procedure forces the surrounding nodes to support the load as the plastically deforming node cannot support any further load resulting in increase in contact area. It has long been accepted that the yielding pressure is generally found to be 2.8 times the yield strength [44] of the material. Eventually, all the plastically deforming nodes, within the contact, will form a plane. A similiar approach was used by Sahlin et al

[45] to develop an elastic-perfectly plastic model under mixed lubrication. A dry contact model was actually used by assuming that only the solid contact causes plastic deformation. Their model requires the application of complementarity condition and is not a true plastoelastohydrodynamic lubrication (PEHL) model.

The PEHL model applied in the current study has been presented in detail by the present authors [40] previously. Here, only brief discussion is presented on the key concepts involved. The Reynolds solver is modified. If the load exceeds the yielding pressure of the material then the load is limited. This limit is applied inside the load balance condition within the mixed lubrication solver. This means that the ability of a node to carry load is limited to the average yielding pressure and these nodes are considered to float i.e. no further load can be supported by these nodes unless the pressure at these nodes falls below the average yielding pressure value. This is achieved by limiting the pressure values during the summation in equation 8 to the yielding pressure i.e. $\forall P \geq P_y, P = P_y$. This summation is used to update the undeformed film thickness value, h_o in equation 2. Therefore, the film thickness values are modified through successive iterations from purely elastic to elasto-plastic values. This process gets repeated as it is a part of the pressure and film thickness convergence loops.

Once the pressure and film thickness have converged, the nodal pressures are truncated to the average yielding pressure and the reduced elastic deformation is calculated using these truncated pressures. The plastic deformation magnitude is evaluated by subtracting this new film thickness for all the plastically deforming nodes from the minimum value of the new film thickness among the elastically deforming nodes. The truncated pressure is then given as initial guess to the EHL solver and the Reynolds solver is again used to get the new pressure profile and film thickness. In this way, by repeating this process, the solution moves from purely elastic to elasto-plastic until a converged is achieved. More details on the method can be found in [40] and [37].

It should be noted that the algorithm works irrespective of whether the tribofilm is present or absent on the substrate material. For the substrate material, a hardness value of 4 GPa was used while for the tribofilm of maximum thickness, a hardness value of 2 GPa was assumed. The hardness was assumed to vary linearly between these values due to tribofilm growth.

2.3. Tribochemistry model

At the tribological contact, frictional energy is generated due to localized shear stress. This energy accelerates the chemical reactions at the interface to form tribochemical layer. The formation of tribofilm has been linked to

several mechanisms, like flash temperatures rise [46], pressure [47], triboe-mission [48] and surface catalysis [49]. The most recent consensus is that the formation of ZDDP tribofilms is a stress promoted thermal activation phe-nomenon which means that the shear stress at the interface reduces the effec-tive forward activation energy of a chemical reaction. Several attempts have been made to capture this mechano-chemical film formation within contact mechanics and lubrication simulations [50, 51, 52, 53]. Among these various approaches, the model of Ghanbarzadeh et al. [51] is adopted to simulate the ZDDP tribofilm growth in this study. Their model considers the formation of tribofilms due to thermal as well as mechanical stimuli. It is assumed that the tribofilm grows as a results of chemical reaction between the lubricant ad-ditives and the substrate. A tribochemical reaction rate is introduced based upon the approach of Bulgarevich et al. [54, 55]. The idea was to introduce the importance of mechanical rubbing on chemical reactions. The thermal reaction of tribofilm formation is captured by an Arrhenius type equation. A factor, x_{tribo} is then multiplied with the reaction rate coefficient. This captures the increase in the reaction rate due to mechano-activation. After some mathematical manipulations and considering a second order reaction rate, the tribofilm growth is expressed as:

$$h = h_{max} - h_{max}e^{(-\frac{k_1 T}{h'})x_{tribo}t} \tag{9}$$

where k_1 and h' are the Boltzzman's and Plank's constant while T and t are the asperity flash temperature and time, respectively. Using this equation, the local tribofilm growth can be modelled alongwith the local variation of properties of the interface due to tribofilm build up. It should be stressed that the assumption of second order chemical reaction may not be true as in essence, multiple chemical reactions occur at the interface. Therefore, guess-ing the true order of the tribochemical reactions becomes very difficult. How-ever, the simplifications introduced in this approach provide a good starting point for simulating tribofilm growth in engineering applications.

The parameters h_{max} and x_{tribo} in equation 9 are fitted to experimental data on tribofilm growth. The fitted parameters can be used to simulate tribofilm growth under different loading conditions. The temperature in equation 9 is the flash temperature plus the bulk temperature. The flash temperatures were calculated in the current study based upon slightly mod-ified form of the Jaeger's moving heat source analysis as given in [56].

The removal of tribofilm is also a key part of the model. The tribofilm growth model assumes that the tribofilm formation and removal takes place simultaneously and the net tribofilm thickness is a competition between for-mation and removal of tribofilm. Several studies support this assumption

9

[57, 58]. Another key reason to use the tribofilm growth model from [51] is that the comparative study between tribofilm removal and wear can be performed. An exponential function has been adopted to consider the tribofilm removal. The complete tribofilm growth equation is achieved by adding removal part to equation 9

$$h = h_{max}\big(1 - e^{(-\frac{k_1 T}{h} r)x_{tribo}t}\big) - C_3\big(1 - e^{-c_4 t}\big) \tag{10}$$

The constants C_3 and C_4 are also fitted to experimental data on tribofilm growth. The tribofilm growth model in equation 10 mainly calculates the growth of tribofilm as a dynamic balance between formation and removal of tribofilm but not the wear of the substrate.

2.4. Mechanical properties of the tribofilm

The mechanical properties of the tribofilm are different compared to the substrate material. This fact has been emphasized and physically considered in the current work. The assessment of mechanical properties of the tribofilm have been performed in several studies [59, 60, 61, 62, 63]. Based upon these studies, it can be suggested that the tribolayer properties are load dependent and are different at the surface than near the bulk substrate. To account for this variable hardness, the approach presented by Andersson et al. [50] has been used in the current work. The tribofilm hardness near the bulk substrate is assumed to be 6 GPa. When the tribofilm has its maximum thickness value, the hardness is assumed to be 2 GPa as done in previous studies [51]. This was first implemented by Andersson et al. [50] and then used by Ghanbarzadeh et al. [51]. The key idea is to have the hardness varying with the thickness of the tribofilm as the tribofilm forms. The change in hardness on the local scale changes the plastic deformation behaviour and vice versa.

2.5. Wear and tribolayer

The Archard wear equation is modified and implemented in this study. The contact pressures are fed into this equation to estimate the substrate wear. To scale up the simulation to compare against experiments, the sliding speed and time step needs adjusting. Archard's equation is implemented in the form that it directly gives the localized wear depth.

$$\Delta h(x,y) = \frac{K}{H}P(x,y)\Delta t v \tag{11}$$

where K,H and v are dimensionless Archard's wear coefficient, hardness of the substrate and the sliding speed, respectively. The term $P(x,y)$ is the local discrete pressures. The wear coefficient is evaluated experimentally. In

this work it is assumed, as in [64], that the coefficient of wear is reducing linearly with the increase in film thickness, being maximum when there is no tribofilm to minimum when the tribofilm is at its maximum thickness.

$$K_{tr} = K_{steel} - (K_{steel} - K_{min})\frac{h}{h_{max}} \qquad (12)$$

This formulation of the wear coefficient enables the simulation of antiwear and extreme pressure characteristic of the tribofilm. It is to be noted that the wear modelled in this work is the mild wear and it considers the loss of substrate material due to reaction with the lubricant additives.

3. Numerical details

In this study it is assumed that the tribofilm only forms at the contacting asperities. The mixed lubrication model calculates the contact pressures and film thickness profiles based upon the rough contact. These are used to calculate the tribofilm growth which is added to the corresponding geometry of ball and disc. The geometries for the next iteration have been changed by plastic deformation, wear and the localized tribofilm growth. As the wear modelled is the mild wear. The wear only alters the rough geometry and not the tribofilm. The tribofilm wear is considered through the removal part in 10. The mixed lubrication equations are solved in the non-dimensional form. The area of study is the square area of 0.5 mm by 0.5 mm.

A simplified MTM-SLIM experimental ball-on-disc configuration is simulated. The steel ball has a diameter of 19.05 mm. In the simulations, the wear track radius is taken to be 23 mm. The applied pressure is 1.15 GPa the roughness on the ball and disc is Rq = 20 nm and Rq = 130 nm respectively. The lubricant rolling speed / entrainment speed, Ur, is 0.1 m/s with an SRR value of 5 %. The temperature of the contact is fixed at 80^oC. A Newtonian lubricant with viscosity $\nu = 0.004 Pa.s$ and a pressure viscosity coefficient $\alpha = 14.94 GPa^{-1}$ is lubricating the contact. The equivalent Young's modulus for the interface is E = 229.67 GPa. The tribofilm growth parameters are h_{max} = 200 nm, $x_{tribo} = 1.66 \times 10^{-16}$, C_1 = 0.05432 and C_2 = 0.0004022 taken from [64]. For all the simulation cases presented in this paper, the material yield limit is fixed at 6 GPa for the substrate and 2 GPa for the tribofilm of maximum thickness. A wear coefficient of 5.45×10^{-8} and 5.45×10^{-9} is used for the substrate wear and the wear in the presence of tribofilm of maximum thickness respectively.

The simulation results labelled as "with tribofilm" correspond to the case with the complete tribofilm model active while the simulation results labelled "without tribofilm" correspond to the case where the tribofilm growth model

11

370 alongwith the hardness update are absent. No tribofilm grows and no change in mechanical properties due to tribofilm occurs. The wear coefficient also stays fixed at the substrate wear value.

4. Results and Discussion

The tribofilm growth affects the lubrication performance within the lu-
375 bricated contact. It is expected that the average film thickness (h_c), lambda ratio (λ), contact area ratio, (A_c, the ratio of solid contact to the total Hertzian contact area) and contact load ratio (W_c, the ratio of load carried by the solid contact to the total load) will change throughout the simulation time. A close look at the evolution of these parameters will greatly help in
380 understanding the role of tribofilms in affecting lubrication performance of the contact. This is the first attempt at modelling the interfacial interactions between tribofilm growth and lubrication performance. Therefore, no direct comparison is available and the discussion is mainly based upon the observations of the evolution behaviour of the key lubrication parameters.

385 It is important to redefine some key parameters before presenting the results. The parameters h_{min} (minimum film thickness), h_c and λ have conventionally been used to represent contact quality and performance. In practice, the h_{min} is the key EHL design parameter [65] but under mixed lubrication conditions, this value is always zero. The point where h_{min} occurs is also
390 not fixed in space due to the transient nature of the contact. Moreover, h_c as defined by the Dowson-Hamrock equation [66] is no longer the true representation of the effective lubricant film within the contact. Therefore, in current study, the average of the nodal film thickness values within 2/3 of the Hertzian zone, as defined in [26], is used used as the average central film
395 thickness h_{avg}. Therefore, two different λ values are presented here, λ_{OLD} is the ratio of h_c to composite roughness while the general use of λ parameter refers to the ratio of h_{avg} to the composite roughness. It should be emphasized that both the central film thickness and the composite roughness change throughout the simulation time due to the changes in tribofilm thick-
400 ness, wear, plastic deformation and the relative movement of the contacting surfaces. Therefore the lambda ratio is not a static value as used in practice.

The first set of results is presented in figure 1 for the roughness evolution of the ball surface for a simulation of 2 hours experiment. It can be clearly seen that the tribofilm roughens the ball surface and the roughness
405 stays higher throughout the simulation time. It suggests that the tribofilm helps to retain the roughness features by reducing wear and limiting the contact pressures at the interface due to the lower hardness of the tribofilm. During the initial stages, the tribofilm growth is fast with minimal removal.

12

The wear rate is also very high during the initial stages due to plastic deformation and absence of tribofilm but eventually slows down due to the formation of the tribofilm and the running in of the high asperities due to plastic deformation. The tribofilm thickness soon reaches its mean value due to the dynamic balance between formation and removal. The growth of tribofilm very quickly modifies the mechanical properties of the contact. This is because the hardness of tribofilm is quite low compared to the substrate hardness. Thus, plastic deformation at the interface is facilitated and the maximum pressures are limited. Based upon the calculations, during the first few iterations, the nodal pressure is even higher than 6 GPa at some of the nodes (due to roughness) resulting in the steel yielding. With the growth of tribofilm the yielding pressure is reduced to values between 6 GPa and 2 GPa and finally close to 2 GPa towards the end of simulation. Thus, the contact transits from substrate yielding to the tribofilm yielding with time.

The λ_{OLD} based upon the conventional h_c is plotted in figure 2. The h_c value used is obtained from Hamrock and Dowson formulations [66] and is a fixed value while the roughness values are the composite roughness values of the contact pair. Figure 2 suggests that the mean roughness keeps decreasing throughout the simulation time as evidenced by the increase in λ_{OLD}. Based upon the conventional understanding and also seen in figure 1, the tribofilm roughens the contact and therefore the λ_{OLD} is always smaller when the tribofilm is present. Therefore, suggesting a reduction in lubrication performance due to presence of tribofilm.

It was pointed out earlier that h_c, defined conventionally, does not truly represent the true lubricant film thickness within the contact. Thus, in figure 3, the h_{avg} is plotted throughout the simulation time, both with and without the presence of tribofilm. It can be readily pointed out that with the tribofilm present, the h_{avg} stays higher throughout the simulation time and the growth of tribofilm roughens both the counterparts. The thicker h_{avg} suggests an improvement in the lubication performance while the roughness increase is expected to degrade lubrication performance. To analyse the comparative influence of both h_{avg} and composite roughness, the ratio of these two quantities, i.e. the λ ratio is plotted in figure 4. It can be seen that the lambda ratio stays higher throughout the simulation time when the tribofilm is present signifying improvement in lubrication performance. Thus, the roughness increase with the presence of tribofilm also helps to retain more lubricant within the contact by forming cavities / pockets of fluid within the contact.

The flow through the contact can be visualized by looking at the film thickness profiles given in figure 7. The profiles have been drawn at X = 0 within the Hertzian contact zone. It can be seen that through the middle

13

region of the contact, the overall film thickness values are thicker when the contact evolves with the tribofilm growth model. A close look at figure 7 indicates that pockets of lubricant film are thicker when tribofilm is present.

To illustrate the entrapment of lubricant within the surface, bearing area curves (BAC) are plotted. The BAC are used to analyse the load carrying surfaces and represent the distribution of material graphically. The bearing area evolution is presented in figure 8. The curve also shows the BAC for the initial starting surface and the BAC of the final worn surface with and without tribofilm. It can be seen that the material ratio for the region with peaks, as shown by the positive part of the curves is almost the same for both surfaces but the region representing the valleys, the negative part of the BAC curves, shows oil retention or lubricant entrapment due to deep valleys. The area on the right side of the curves below the zero line has increased by the presence of tribofilm, signifying valley volume which is proportional to oil retention.

Next, the results on the wear of the disc (rough) surface are presented in figure 6. The final wear depth of the worn surface is 152 nm without the tribofilm and $\approx$ 132 nm when the tribofilm growth is considered. The predicted average wear depth values are smaller in the current study but agree well with experimental values of wear depth from Ghanbarzadeh et al. [64] from which the parameters for the tribofilm growth model were taken. It can be seen that the wear is reduced with tribofilm. The evolution of wear is a complex result of the interplay between plastic deformation, wear and tribofilm growth. It can be seen that the wear rate also changes throughout the simulation time.

The simulation results presented in this paper provide new insights into the action of the antiwear additive ZDDP. The antiwear film not only reduces wear due to the formation of chemical layers but the physical presence of the tribofilm is also expected to play a significant role in reducing wear. It can be seen that the lambda ratio decreases in both the cases (see figure 4) but when the tribofilm is present, the degradation of the lambda ratio is delayed. Also the rate of decrease in the lambda ratio decreases with time and its final values can be related to the steady state wear rate of the tribochemically active system.

The change in the mechanics of the contact due to tribofilm growth is even more interesting. The A_c and W_c evolution in figure 5 shows that both these parameters stay higher when the tribofilm growth is included into the simulation model. Thus, the growth of tribofilm not only result in increased roughness but also increases the area supported by the dry / tribofilm regions and the load carried by this dry / tribofilm region is also higher compared to when tribofilm growth is not included into the simulations. The increase

14

in contact area ratio may also be linked to the fact that the tribofilm is compliant and thus, undergoes yielding easily compared to the substrate. The friction in contacts is directly proportional to the contact area ratio. Therefore, the increase in contact area ratio may also be linked to the increase in friction as more dry contact nodes within the Hertzian contact zone mean more dry friction. A closer look at both the plots in figure 5 suggests that the contact area ratio keeps on decreasing but the contact load ratio decreases and reaches a limiting value.

Only the starting value of λ is given in experimental results as well as numerical studies. In reality, however, the λ and h_c change significantly throughout the experiments due to the change in the roughness, wear, plastic deformation, tribofilm growth. It has not been possible until now to study the effects of tribofilm build up on the lubrication performance due to the inability of experiments to capture detailed information about the contact. On the other hand, simulation studies in lubrication science have not been able to capture the effect of tribofilm due to not being able to capture the lubrication, contact mechanics and tribochemistry in a single framework. The results from the current study suggest that the model developed effectively merges the lubrication science with tribochemistry.

The extension of the modelling capabilities to include tribochemical effects has not received much attention yet. The potential reason behind this can be the difficulties in defining asperity contact within the continuum restrictions. Boundary lubrication is defined as the state where contact characteristics are dominated by asperity contacts and the state of contact is considered as the absence of any lubricant / hydrodynamic film. It is to be noted that the dry contact condition is defined using continuum principles and the contacts are rough at the atomic scale where the atomic interactions control interfacial chemical phenomenon. The limitations on the use of continuum models to describe contact mechanics were discussed by Luan and Robbins [67]. They suggest that the continuum assumption breaks down as the atomic dimensions are reached. The lubricant also loses its continuum nature and starts to dissociate at the interface as suggested by the work of Spikes [68] and Luo et al. [69] and recently pointed out by Zhu and Wang [36]. Thus, the unified mixed lubrication models are not suitable for representing any atomic scale events in their conventional implementations. Some studies using molecular dynamics simulations have started to appear [70, 71] but these are limited to fundamental understanding of the interfacial phenomenon. In the current study, the continuum restriction was bypassed by considering an approximate model for tribofilm growth.

15

Conclusion

The tribochemical mixed lubrication model developed earlier by the authors [37] was used to study the effects of tribofilm growth on lubricaiton parameters. The tribofilm growth was found to have significant effect on the lubricaiton parameters. The roughness of the contact pair increases with the presence and growth of tribofilm. This roughness increase was found to retain more lubricant within the pockets formed by rough surface contact. Thus, thicker lubricant films can be sustained. The lambda ratio was found to stay higher with the growth of tribofilm on the contacting surfaces and a new mechanism for the action of the ZDDP antiwear films in reducing wear was proposed. Thus, it can be concluded that the ZDDP tribofilm performs its antiwear action not only due to its chemical film formation but also due to its physical presence by helping to retain more lubricant within the contact.

5. Acknowledgement

References

[1] H Spikes. The history and mechanisms of zddp. *Tribology letters*, 17(3):469–489, 2004.

[2] A. Dorgham, A. Azam, A. Morina, and A. Neville. On the transient decomposition and reaction kinetics of zinc dialkyldithiophosphate. *ACS applied materials & interfaces*, 2018.

[3] A. Dorgham, P. Parsaerian, A. Azam, C. Wang, A. Morina, and A. Neville. Single-asperity study of the reaction kinetics of p-based triboreactive films. *Tribology International*, 2018.

[4] A I Petrusevich. *Principal conclusions from contact-hydrodynamic theory of lubrication.* Associated Technical Services, 1950.

[5] AP Ranger, CMM Ettles, and A Cameron. The solution of the point contact elasto-hydrodynamic problem. In *Proceedings of the Royal Society of London A: Mathematical, Physical and Engineering Sciences*, volume 346, pages 227–244. The Royal Society, 1975.

[6] B J Hamrock and D Dowson. Isothermal elastohydrodynamic lubrication of point contacts. 1: Theoretical formulation. 1975.

[7] B J Hamrock and D Dowson. Isothermal elastohydrodynamic lubrication of point contacts: part iiifully flooded results. *Journal of Lubrication Technology*, 99(2):264–275, 1977.

[8] CJ Hooke. The elastohydrodynamic lubrication of heavily loaded point contacts. *Journal of Mechanical Engineering Science*, 22(4):183–187, 1980.

[9] HP Evans and RW Snidle. Inverse solution of reynolds equation of lubrication under point-contact elastohydrodynamic conditions. *Journal of Lubrication Technology*, 103(4):539–546, 1981.

[10] HP Evans and RW Snidle. The elastohydrodynamic lubrication of point contacts at heavy loads. In *Proceedings of the Royal Society of London A: Mathematical, Physical and Engineering Sciences*, volume 382, pages 183–199. The Royal Society, 1982.

[11] D Zhu and S Wen. A full numerical solution for the thermoelastohydrodynamic problem in elliptical contacts. *Journal of tribology*, 106(2):246–254, 1984.

17

[12] K H Kim and F Sadeghi. Three-dimensional temperature distribution in ehd lubrication: part icircular contact. *Journal of tribology*, 114(1):32–41, 1992.

[13] CH VENNER. Multilevel solution of the ehl line and point contact problems(ph. d. thesis). 1991.

[14] X Ai. Numerical analyses of elastohydrodynamically lubricated line and point contacts with rough surfaces by using semi-system and multigrid methods (volumes 1 and 2). 1993.

[15] GCHH Nijenbanning, CH Venner, and H Moes. Film thickness in elastohydrodynamically lubricated elliptic contacts. *Wear*, 176(2):217–229, 1994.

[16] CH Venner and AA Lubrecht. Multigrid techniques: a fast and efficient method for the numerical simulation of elastohydrodynamically lubricated point contact problems. *Proceedings of the Institution of Mechanical Engineers, Part J: Journal of Engineering Tribology*, 214(1):43–62, 2000.

[17] D Jalali-Vahid, H Rahnejat, and ZM Jin. Elastohydrodynamic solution for concentrated elliptical point contact of machine elements under combined entraining and squeeze-film motion. *Proceedings of the Institution of Mechanical Engineers, Part J: Journal of Engineering Tribology*, 212(6):401–411, 1998.

[18] Y Liu, S Wang, Q Jand Bair, and P Vergne. A quantitative solution for the full shear-thinning ehl point contact problem including traction. *Tribology Letters*, 28(2):171–181, 2007.

[19] AD Chapkov, S Bair, P Cann, and AA Lubrecht. Film thickness in point contacts under generalized newtonian ehl conditions: numerical and experimental analysis. *Tribology International*, 40(10):1474–1478, 2007.

[20] P Kumar and MM Khonsari. Ehl circular contact film thickness correction factor for shear-thinning fluids. *Journal of Tribology*, 130(4):041506, 2008.

[21] P Kumar and MM Khonsari. On the role of lubricant rheology and piezoviscous properties in line and point contact ehl. *Tribology international*, 42(11):1522–1530, 2009.

18

[22] P Katyal and P Kumar. Central film thickness formula for shear thinning lubricants in ehl point contacts under pure rolling. *Tribology International*, 48:113–121, 2012.

[23] D Zhu and HS Cheng. Effect of surface roughness on the point contact ehl. *Journal of tribology*, 110(1):32–37, 1988.

[24] L Chang. A deterministic model for line-contact partial elastohydrodynamic lubrication. *Tribology international*, 28(2):75–84, 1995.

[25] X Jiang, DY Hua, HS Cheng, X Ai, and S C Lee. A mixed elastohydrodynamic lubrication model with asperity contact. *Journal of tribology*, 121(3):481–491, 1999.

[26] D Zhu and YZ Hu. The study of transition from elastohydrodynamic to mixed and boundary lubrication. *The advancing frontier of engineering tribology, Proceedings of the 1999 STLE/ASME HS Cheng Tribology Surveillance*, pages 150–156, 1999.

[27] MJA Holmes, HP Evans, and RW Snidle. Analysis of mixed lubrication effects in simulated gear tooth contacts. In *ASME/STLE 2004 International Joint Tribology Conference*, pages 447–457. American Society of Mechanical Engineers, 2004.

[28] S Li and A Kahraman. A mixed ehl model with asymmetric integrated control volume discretization. *Tribology International*, 42(8):1163–1172, 2009.

[29] Y Liu, Q J Wang, W Wang, YZ Hu, and D Zhu. Effects of differential scheme and mesh density on ehl film thickness in point contacts. *Journal of Tribology*, 128(3):641–653, 2006.

[30] WZ Wang, H Wang, YC Liu, YZ Hu, and D Zhu. A comparative study of the methods for calculation of surface elastic deformation. *Proceedings of the Institution of Mechanical Engineers, Part J: Journal of Engineering Tribology*, 217(2):145–154, 2003.

[31] D Zhu. On some aspects of numerical solutions of thin-film and mixed elastohydrodynamic lubrication. *Proceedings of the Institution of Mechanical Engineers, Part J: Journal of Engineering Tribology*, 221(5):561–579, 2007.

[32] WZ Wang, YZ Hu, YC Liu, and D Zhu. Solution agreement between dry contacts and lubrication system at ultra-low speed. *Proceedings of*

<div style="margin-left: 2em; text-indent: -2em;">

the *Institution of Mechanical Engineers, Part J: Journal of Engineering Tribology*, 224(10):1049–1060, 2010.

[33] WZ Wang, S Li, D Shen, S Zhang, and YZ Hu. A mixed lubrication model with consideration of starvation and interasperity cavitations. *Proceedings of the Institution of Mechanical Engineers, Part J: Journal of Engineering Tribology*, 226(12):1023–1038, 2012.

[34] Retainers Stamped From Steel. The finite journal bearing, considering vaporization.

[35] Harold G Elrod. A cavitation algorithm. *Trans. ASME, J. Lubr. Technol.*, 103(3):350, 1981.

[36] D Zhu and Q J Wang. Elastohydrodynamic lubrication: a gateway to interfacial mechanicsreview and prospect. *Journal of Tribology*, 133(4):041001, 2011.

[37] A Azam, A Ghanbarzadeh, A Neville, A Morina, and M CT Wilson. Modelling tribochemistry in the mixed lubrication regime. *Tribology International*, 2018.

[38] A Azam. *Modelling interfacial tribochemistry in the mixed lubrication regime*. PhD thesis, University of Leeds, 2018.

[39] YZ Hu and K Tonder. Simulation of 3-d random rough surface by 2-d digital filter and fourier analysis. *International Journal of Machine Tools and Manufacture*, 32(1-2):83–90, 1992.

[40] A. Azam, A. Dorgham, A. Morina, A. Neville, and Mark C.T. Wilson. A simple deterministic plastoelastohydrodynamic lubrication (pehl) model in mixed lubrication. *Tribology International*, 131:520–529, 2019.

[41] YZ Hu and D Zhu. A full numerical solution to the mixed lubrication in point contacts. *Journal of Tribology*, 122(1):1–9, 2000.

[42] R Gohar. *Elastohydrodynamics*. World Scientific, 2001.

[43] S Liu, Q Wang, and G Liu. A versatile method of discrete convolution and fft (dc-fft) for contact analyses. *Wear*, 243(1):101–111, 2000.

[44] KL Johnson. Contact mechanics cambridge univ. *Press, Cambridge*, 1985.

</div>

[45] F Sahlin, R Larsson, A Almqvist, PM Lugt, and P Marklund. A mixed lubrication model incorporating measured surface topography. part 1: theory of flow factors. *Proceedings of the Institution of Mechanical Engineers, Part J: Journal of Engineering Tribology*, 224(4):335–351, 2010.

[46] Z. Yin, M. Kasrai, M. Fuller, G. M. Bancroft, K. Fyfe, and K. H. Tan. Application of soft x-ray absorption spectroscopy in chemical characterization of antiwear films generated by zddp part i: the effects of physical parameters. *Wear*, 202(2):172–191, 1997.

[47] N. J Mosey, M. H. Müser, and T. K. Woo. Molecular mechanisms for the functionality of lubricant additives. *Science*, 307(5715):1612–1615, 2005.

[48] C. Kajdas, R. Tummler, H. von Ardenne, and W. Schwarz. The relevance of negative ion mass spectroscopy to the interpretation of the reaction of metal dialkyldithiophosphates during lubricated rubbing. *ZFI Mitteilungen*, 115:107–112, 1986.

[49] J Zhang and H Spikes. On the mechanism of zddp antiwear film formation. *Tribology Letters*, 63(2):1–15, 2016.

[50] J Andersson, R Larsson, A Almqvist, M Grahn, and I Minami. Semi-deterministic chemo-mechanical model of boundary lubrication. *Faraday discussions*, 156(1):343–360, 2012.

[51] A Ghanbarzadeh, M Wilson, A Morina, D Dowson, and A Neville. Development of a new mechano-chemical model in boundary lubrication. *Tribology International*, 93:573–582, 2016.

[52] A. Akchurin and R. Bosman. A deterministic stress-activated model for tribo-film growth and wear simulation. *Tribology Letters*, 65(2):59, 2017.

[53] V Brizmer, C Matta, I Nedelcu, and GE Morales-Espejel. The influence of tribolayer formation on tribological performance of rolling/sliding contacts. *Tribology Letters*, 65(2):57, 2017.

[54] S. B. Bulgarevich, M. V. Boiko, V. I. Kolesnikov, and V. A. Feizova. Thermodynamic and kinetic analyses of probable chemical reactions in the tribocontact zone and the effect of heavy pressure on evolution of adsorption processes. *Journal of Friction and Wear*, 32(4):301–309, 2011.

[55] S. B. Bulgarevich, M. V. Boiko, V. I. Kolesnikov, and K. E. Korets. Population of transition states of triboactivated chemical processes. *Journal of Friction and Wear*, 31(4):288–293, 2010.

[56] L Chang and YR Jeng. A mathematical model for the mixed lubrication of non-conformable contacts with asperity friction, plastic deformation, flash temperature, and tribo-chemistry. *Journal of Tribology*, 136(2):022301, 2014.

[57] YC Lin and H So. Limitations on use of zddp as an antiwear additive in boundary lubrication. *Tribology International*, 37(1):25–33, 2004.

[58] A. Morina and A. Neville. Understanding the composition and low friction tribofilm formation/removal in boundary lubrication. *Tribology International*, 40(10):1696–1704, 2007.

[59] S Bec, A Tonck, JM Georges, RC Coy, JC Bell, and GW Roper. Relationship between mechanical properties and structures of zinc dithiophosphate anti–wear films. In *Proceedings of the Royal Society of London A: Mathematical, Physical and Engineering Sciences*, volume 455, pages 4181–4203. The Royal Society, 1999.

[60] G Nehme, R Mourhatch, and P B Aswath. Effect of contact load and lubricant volume on the properties of tribofilms formed under boundary lubrication in a fully formulated oil under extreme load conditions. *Wear*, 268(9):1129–1147, 2010.

[61] M Aktary, M T McDermott, and Gerald A McAlpine. Morphology and nanomechanical properties of zddp antiwear films as a function of tribological contact time. *Tribology letters*, 12(3):155–162, 2002.

[62] M A Nicholls, T Do, P R Norton, M Kasrai, and G M Bancroft. Review of the lubrication of metallic surfaces by zinc dialkyl-dithiophosphates. *Tribology International*, 38(1):15–39, 2005.

[63] R Mourhatch and P B Aswath. Tribological behavior and nature of tribofilms generated from fluorinated zddp in comparison to zddp under extreme pressure conditionspart ii: morphology and nanoscale properties of tribofilms. *Tribology International*, 44(3):201–210, 2011.

[64] A. Ghanbarzadeh, P. Parsaeian, A. Morina, MCT Wilson, M CP van Eijk, I. Nedelcu, D. Dowson, and A. Neville. A semi-deterministic wear model considering the effect of zinc dialkyl dithiophosphate tribofilm. *Tribology Letters*, 61(1):12, 2016.

[65] A Z Szeri. *Fluid film lubrication.* Cambridge university press, 2010.

[66] B J Hamrock and D. Dowson. Isothermal elastohydrodynamic lubrication of point contacts: Part 1theoretical formulation. *Journal of Lubrication Technology*, 98(2):223–228, 1976.

[67] B Luan and M O Robbins. The breakdown of continuum models for mechanical contacts. *Nature*, 435(7044):929, 2005.

[68] H Spikes. The borderline of elastohydrodynamic and boundary lubrication. *Proceedings of the Institution of Mechanical Engineers, Part C: Journal of Mechanical Engineering Science*, 214(1):23–37, 2000.

[69] J Luo, S Wen, and P Huang. Thin film lubrication. part i. study on the transition between ehl and thin film lubrication using a relative optical interference intensity technique. *Wear*, 194(1-2):107–115, 1996.

[70] A Martini, Y Liu, RQ Snurr, and QJ Wang. Molecular dynamics characterization of thin film viscosity for ehl simulation. *Tribology Letters*, 21(3):217–225, 2006.

[71] P Z Zhu, Y Z Hu, T B Ma, and H Wang. Molecular dynamics study on friction due to ploughing and adhesion in nanometric scratching process. *Tribology Letters*, 41(1):41–46, 2011.
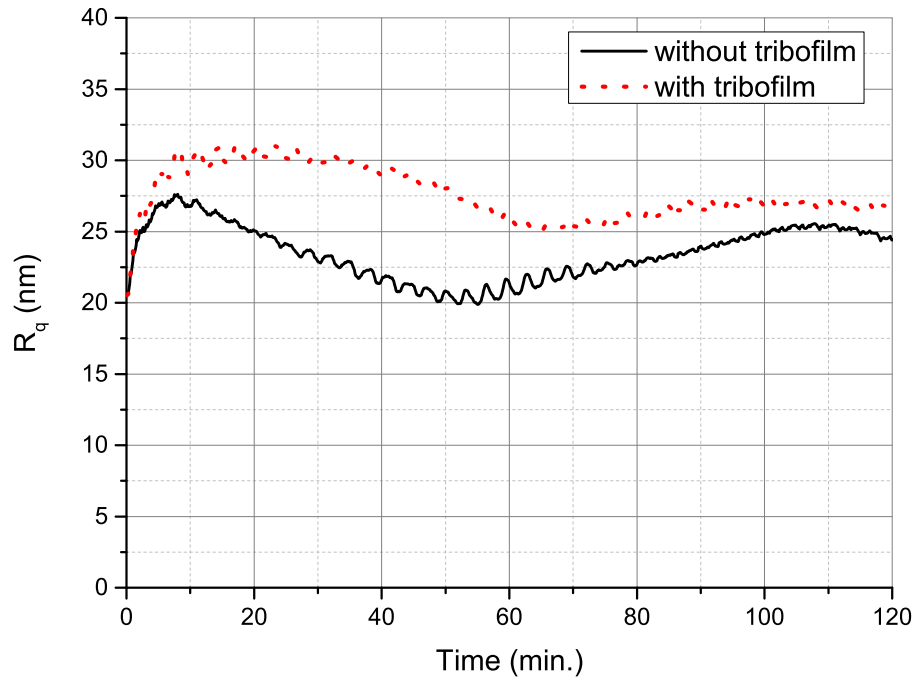
Figure 1: Roughness evolution on the ball surface (smoother counterpart)
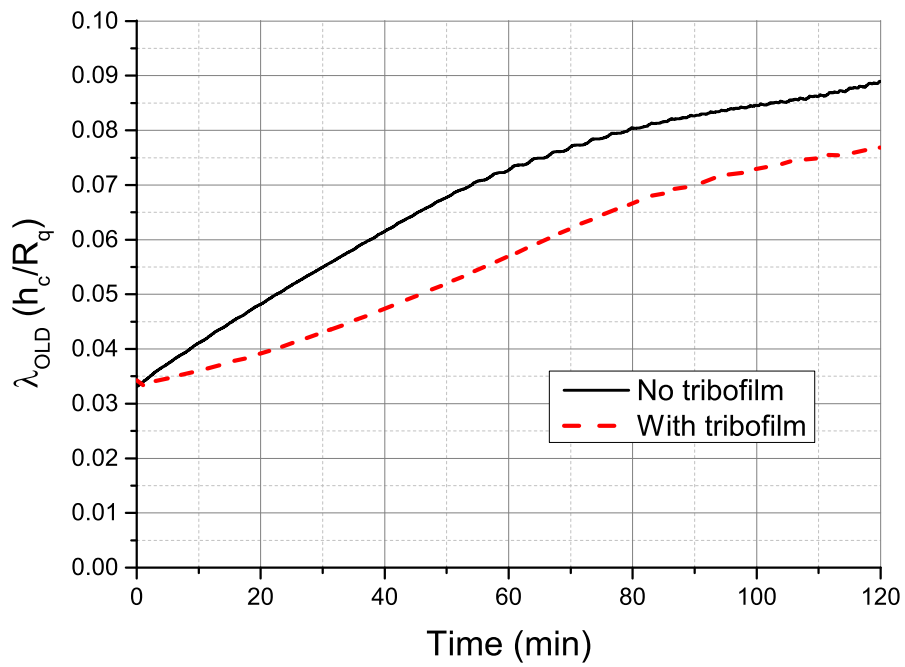
Figure 2: The evolution of lambda ratio. The central film thickness is based upon the Hamrock and Dowson [66] formulation and the roughness is the composite root mean square roughness of the contact pair.
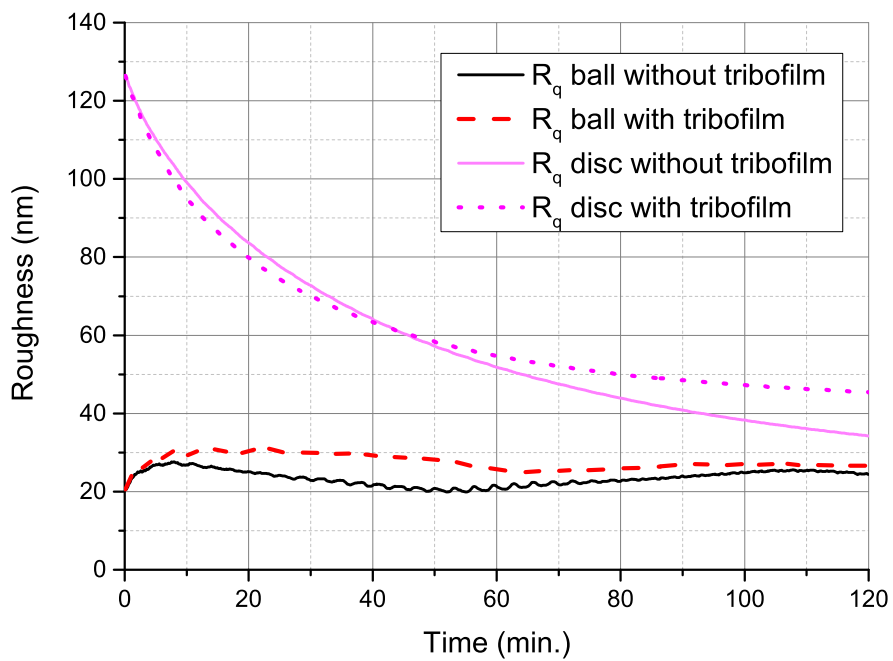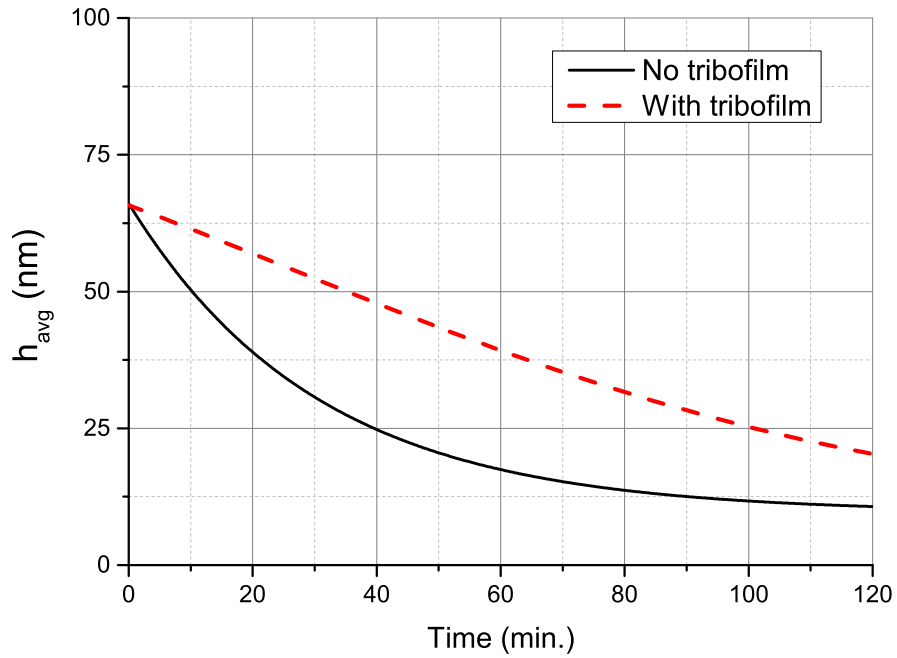
Figure 3: Top: The evolution of the average film thickness inside the contact. Bottom: The evolution of the root mean square roughnes on both the counterparts.
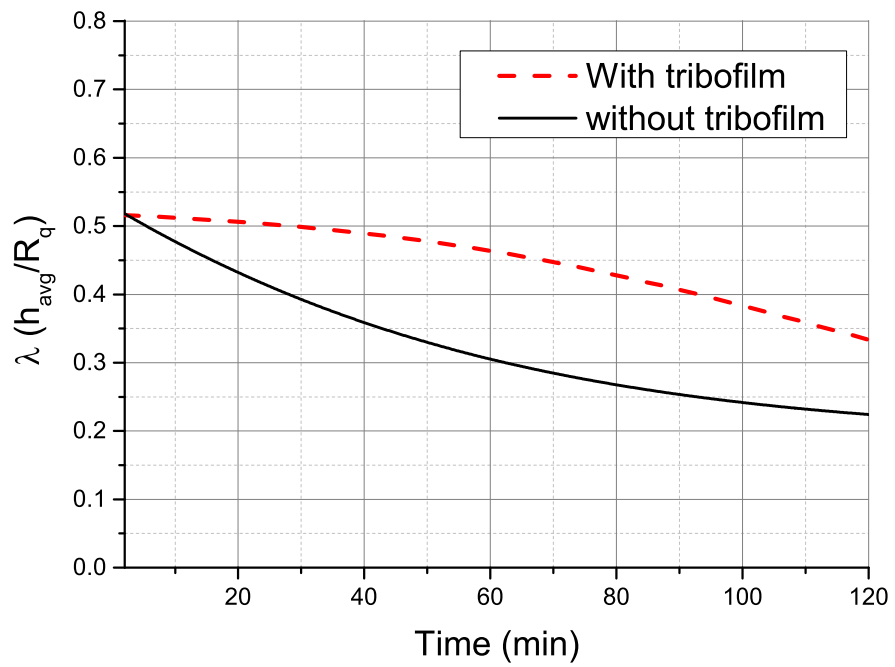
Figure 4: The evolution of lambda ratio. The central film thickness is average of the nodal film thickness values within 2/3 of the Hertzian contact zone and the roughness is the composite root mean square roughness of the contact pair.
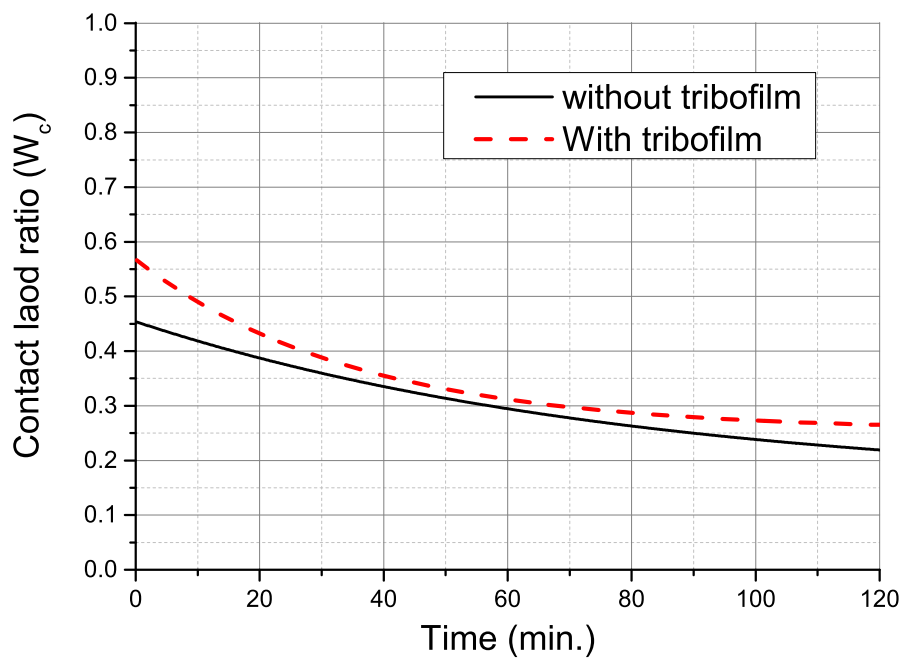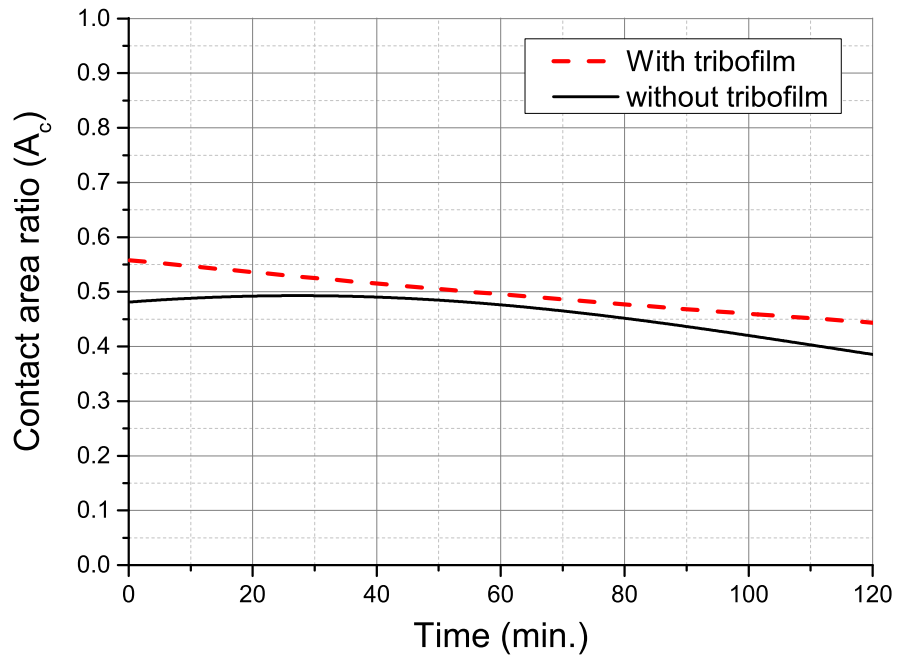
Figure 5: Top: The evolution of the contact area ratio with time. Bottom: The evolution of the contact load ratio with time.
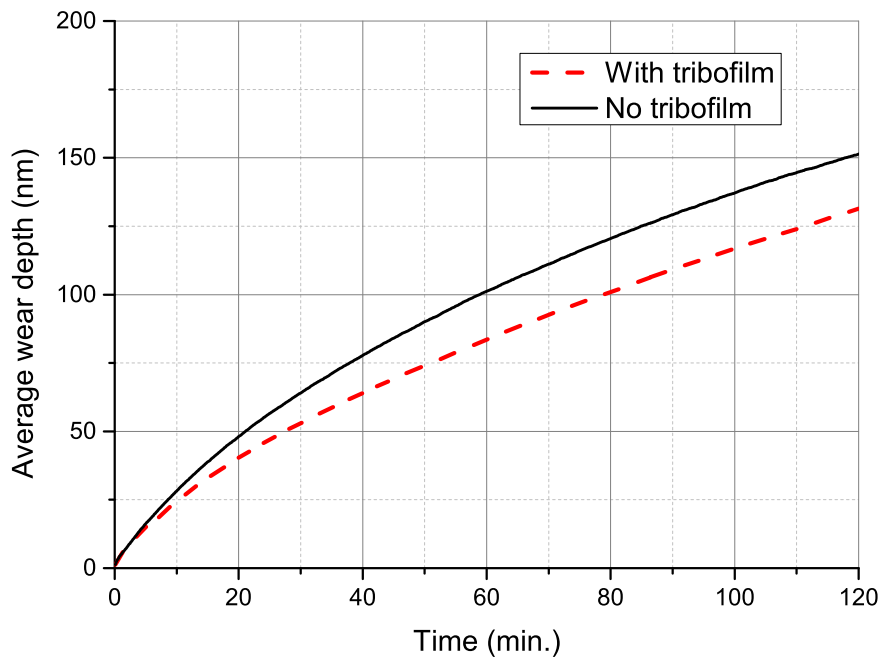
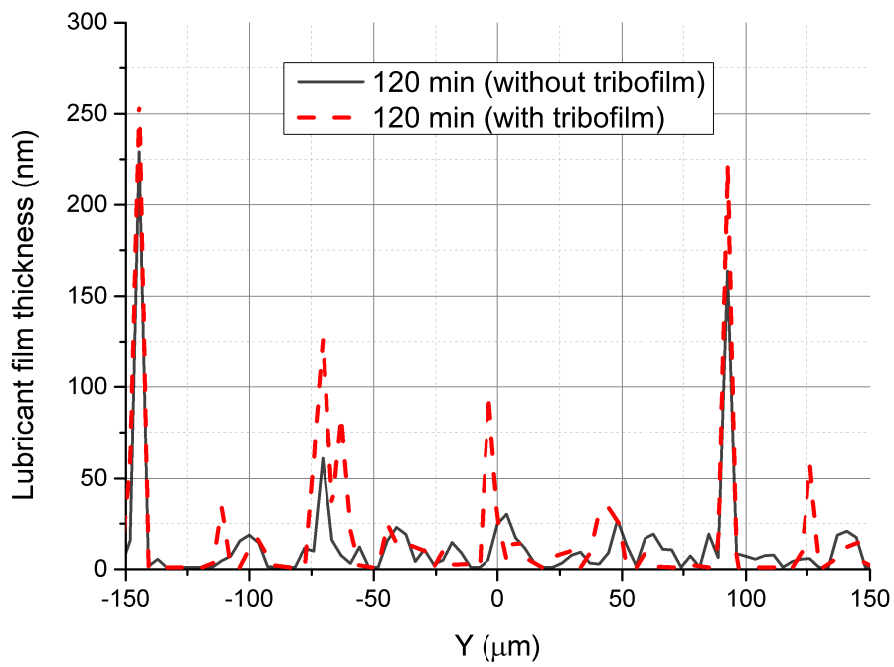Figure 6: The evolution of the wear with time. The presence of tribofilm results in lower wear.

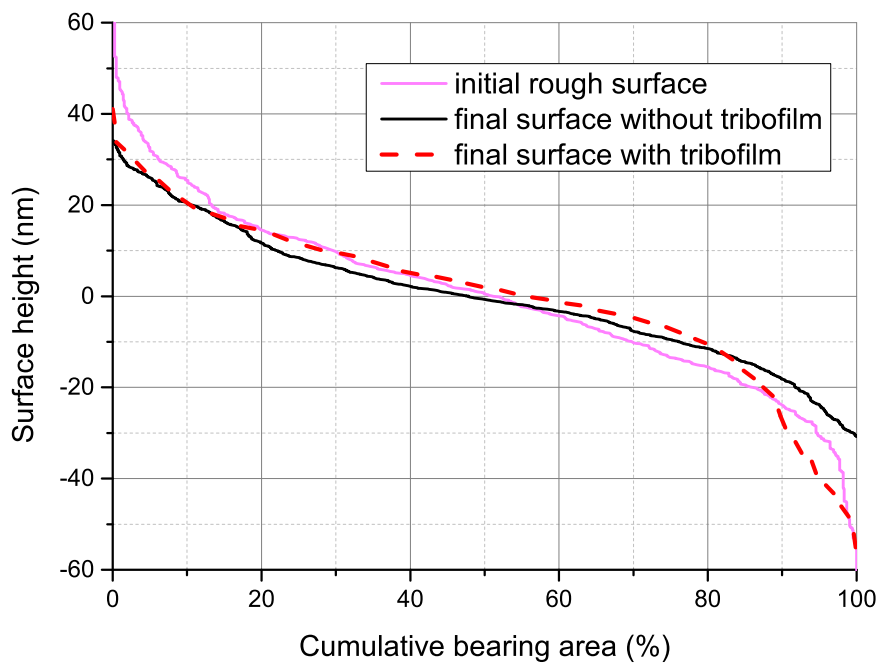Figure 7: The final film thickness profile at X = 0 within the Hertzian contact zone. The presence of tribofilm results in thicker overall lubricant film.

Figure 8: The bearing area curve (BAC) evolution.